

Article

Not peer-reviewed version

---

# Unlocking Tyrosinase Inhibition: Insights from Molecular Dynamics and Binding Free Energy Studies of Novel Arylpiperidine and Arylpiperazine-Based Inhibitors

---

Lucas Sousa Martins , Beatriz Alves Bentes , [Jerônimo Lameira](#) <sup>\*</sup> , [José Rogério Araújo Silva](#) <sup>\*</sup>

Posted Date: 29 August 2023

doi: 10.20944/preprints202308.1873.v1

Keywords: Tyrosinases; Melanogenesis; Inhibitors, Computational Analysis; van der Waals interactions



Preprints.org is a free multidiscipline platform providing preprint service that is dedicated to making early versions of research outputs permanently available and citable. Preprints posted at Preprints.org appear in Web of Science, Crossref, Google Scholar, Scilit, Europe PMC.

Copyright: This is an open access article distributed under the Creative Commons Attribution License which permits unrestricted use, distribution, and reproduction in any medium, provided the original work is properly cited.

## Article

# Unlocking Tyrosinase Inhibition: Insights from Molecular Dynamics and Binding Free Energy Studies of Novel Arylpiperidine and Arylpiperazine-Based Inhibitors

Lucas Sousa Martins <sup>1</sup>, Beatriz Alves Bentes <sup>1</sup>, Jerônimo Lameira <sup>1,\*</sup> and José Rogério A. Silva <sup>1,2,\*</sup>

<sup>1</sup> Laboratory of Computer Modeling of Molecular Biosystems, Federal University of Pará, Belém 66075-110, Pará, Brazil

<sup>2</sup> Catalysis and Peptide Research Unit, University of KwaZulu-Natal, Durban 4000, South Africa

\* Correspondence: lameira@ufpa.br, rogerio@ufpa.br

**Abstract:** Tyrosinases (TYR) play an important role in oxidizing phenols and catechols, leading to the formation of catechols and ortho-quinones, respectively. In mammals, TYR catalyzes the conversion of L-Tyrosine to quinone, a pivotal step in melanogenesis, which generates melanin pigments responsible for protecting against UV radiation and oxidative stress. Given TYR's importance in melanin-related disorders and cosmetic applications, the inhibition of TYR has garnered attention for controlling melanin production. However, current inhibitors like hydroquinone, arbutin, and kojic acid (KA) have limitations in terms of side effects and effectiveness. A novel class of TYR inhibitors featuring arylpiperidine and arylpiperazine components has demonstrated potent inhibitory activity. This study presents a computational analysis of these inhibitors using molecular docking, molecular dynamics (MD) simulations, and the Linear Interaction Energy (LIE) method was used to estimate binding free energies. The arylpiperidine and arylpiperazine inhibitors exhibit remarkable stability within the TYR active site during simulations. The van der Waals interactions are notably sustained, indicating effective inhibition mechanisms. The results from LIE calculations closely align with experimental binding affinities. In summary, these results contribute to the understanding of TYR inhibition and underscore the potential of arylpiperidine and arylpiperazine derivatives as effective agents for modulating melanin production in both cosmetic and pharmaceutical applications. Overall, this study sheds light on the intricate interactions between inhibitors and TYR, opening avenues for the development of novel therapies and interventions.

**Keywords:** Tyrosinases; melanogenesis; inhibitors; computational analysis; van der Waals interactions

## Introduction

Melanin holds significant importance across various organisms, serving crucial roles like photoprotection, thermoregulation, and wound healing. In humans, this pigment dictates the color of skin, eyes, and hair. [1–3]. In this biological pathway, the resultant melanin pigments assume a key role, serving as a formidable defense mechanism against the detrimental effects of UV radiation and the perilous onslaught of free radicals, thereby safeguarding the integumentary system from potential harm. [4] On the other hand, abnormal melanin loss and depigmentation can have pronounced aesthetic and dermatological implications. Conversely, elevated melanin production and accumulation are observed in diverse skin disorders, encompassing Parkinson's disease-linked neurodegeneration [5] and a heightened risk of skin cancer [6]. Indeed, it is widely acknowledged that pathologies associated with melanin can give rise to a spectrum of skin afflictions, encompassing hyperpigmentation, the formation of lesions, and the development of melasma [7,8].

In mammals, Tyrosinase (TYR) assumes a key role in the process of melanogenesis [9]. Then, the inhibition of TYR emerges as a strategic approach to regulate melanin production [10]. Consequently, the pursuit of TYR inhibitors has sparked considerable enthusiasm within the realms of treating skin pathologies and advancing dermocosmetic interventions. Tyrosinases (TYR, EC 1.14.18.1) are

metalloenzymes that abound across a wide spectrum of life forms, encompassing mammals, fungi, bacteria, and plants. These TYRs prominently feature binuclear active sites, characterized by the presence of two copper ions meticulously coordinated by six histidine residues [11]. Their primary catalytic function lies in the oxidation of phenols and catechols, yielding catechols and ortho-quinones, respectively (Figure 1) [9].

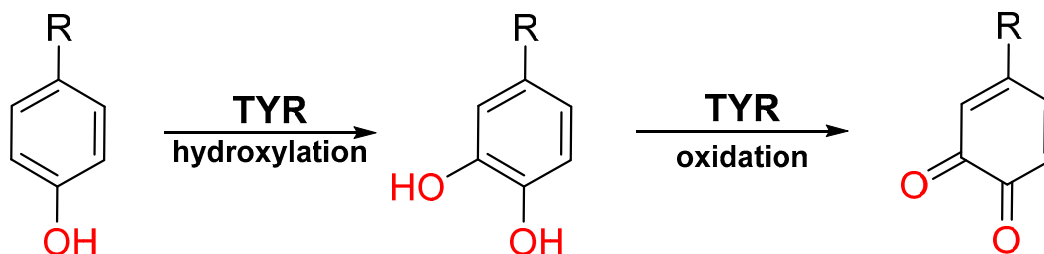


**Figure 1.** General catalytic mechanism scheme of TYR.

Kojic acid (KA) has been employed as a benchmark for assessing TYR inhibition [12–16]. However, it has exhibited adverse effects linked to its pronounced sensitizing potential and substantial toxicity [17,18]. These drawbacks cast a shadow over its suitability for application in the realms of both cosmetics and pharmaceuticals. Additionally, research underscores the pressing need for the formulation of novel TYR inhibitors. Recently, Ferro et al. [19] successfully synthesized a novel class of TYR inhibitors featuring arylpiperidine and arylpiperazine components, demonstrating their effectiveness at micromolar concentrations. Notably, these inhibitors exhibited greater potency when compared to the reference compound, KA. A variety of such inhibitors, exemplified by hydroquinone, arbutin, and KA, presently find application as agents for depigmentation [20,21]. These features underscore the importance of exploring compounds that inhibit melanin synthesis, thereby advancing the development of skin-whitening and depigmenting agents, a pursuit of considerable interest within the cosmetic industry [10].

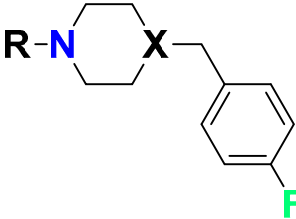
In this study, we present a robust computational analysis of TYR inhibitors that were synthesized and assessed by Ferro et al [19]. This analysis was conducted through the application of molecular docking, molecular dynamics (MD) simulations, and calculations of binding free energy [22]. Our investigation sheds light on the mechanism of TYR inhibition by furnishing structural and energetic insights that align with experimental findings. Furthermore, it is important to note that all computational methodologies employed in this study have undergone rigorous validation by our research group [23–27].

## Computational Methods

### *Molecular Docking and Molecular Dynamics (MD) simulations*

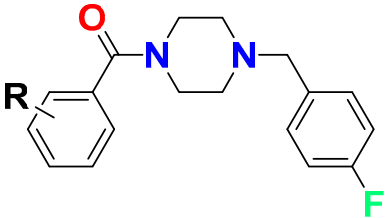
The crystal structures of TYR from *Bacillus megaterium* (TYRBm) were obtained from the Protein Data Bank (PDB codes 5OAE and 6EI4) as well as the arylpiperidine and arylpiperazine-based compounds (Tables 1 and 2) [19]. Molecular docking calculations were conducted using Molegro Virtual Docker (MVD) version 5.5 [28], a tool that has proven effective in TYR systems [23–27]. Specifically, for the docking procedures, Cu<sup>2+</sup> ions were represented as van der Waals spheres positioned within the catalytic site of TYR. Our research group has successfully utilized the MVD program to elucidate the binding modes of TYR inhibitors in previous studies [23–27]. Consequently, the same computational procedures were applied to the selected TYR systems. Detailed equations for the MOLDOCK method can be found elsewhere [28].

**Table 1.** Arylpiperidine (L02–L07) and arylpiperazine-based (L08–L12) inhibitors of TYR evaluated by Ferro et al. [19] and their respective experimental binding free energy ( $\Delta G_{EXP}$ ), at 310 K, from IC<sub>50</sub> values, according eq. 2.



Inhibitor	R	X	$\Delta G_{EXP}$ (kcal/mol)
L02	CH <sub>3</sub> CH <sub>2</sub>	CH	-5.58
L03	CH <sub>3</sub> CO	CH	-6.53
L04	H	CH	-5.02
L05	CH <sub>3</sub> CH <sub>2</sub> CO	CH	-6.55
L06	CH <sub>3</sub> CH(CH <sub>3</sub> )CO	CH	-6.32
L07	C <sub>6</sub> H <sub>5</sub> CO	CH	-6.68
L08	H	N	-5.77
L09	CH <sub>3</sub> CO	N	-6.15
L10	CH <sub>3</sub> CH <sub>2</sub> CO	N	-6.09
L11	CH <sub>3</sub> CH(CH <sub>3</sub> )CO	N	-6.40
L12	C <sub>6</sub> H <sub>5</sub> CO	N	-6.91

**Table 2.** Arylpiperazine-based inhibitors of TYR evaluated by Ferro et al. [19] and their respective experimental binding free energy ( $\Delta G_{EXP}$ ), at 310 K, from IC<sub>50</sub> values, according eq. 2.



Inhibitor	R	$\Delta G_{EXP}$ (kcal/mol)
L13	2-F	-7.70
L14	3-F	-6.05

L15	4-F	-7.25
L16	2-CH <sub>3</sub>	-7.49
L17	3-CH <sub>3</sub>	-5.33
L18	4-CH <sub>3</sub>	-6.35
L19	2-OCH <sub>3</sub>	-8.07
L20	3-OCH <sub>3</sub>	-6.48
L21	4-OCH <sub>3</sub>	-7.15
L22	2-OH	-7.31
L23	3-OH	-6.95
L24	4-OH	-6.47

For MD simulations, the most favorable docking conformations of TYR inhibitors were chosen as initial configurations. The OPLS-AA [29] and TIP3P [30] force fields were employed to define parameters for the solute (comprising TYR amino acids and its inhibitors) and solvent subsystems, respectively. Parameters for TYR inhibitors were computed using the MACROMODEL package [31,32]. In particular, a set of classical parameters proposed by Liao et al. [33], referred to as the Cu<sup>2+</sup> dummy model (CuDum), was employed to characterize the metal center of TYR*Bm*. The PROPKA approach [34] was used to establish pKa values for all ionizable amino acid (AA) residues at a neutral pH.

Each TYR system was immersed in a simulation sphere with a 20 Å radius, comprised of TIP3P molecules [30], centered at the respective TYR inhibitor's center of mass. The surface-constrained all-atom solvent (SCAAS) method [35] was employed to handle polarization and radial constraints at the surface of the simulation sphere. To account for dielectric screening [36], all ionizable amino acid residues near the sphere boundary were neutralized. A 10 Å cutoff was applied when computing non-bonded interaction energies, with only the atoms of the inhibitors excluded from this calculation. Long-range electrostatic interactions were computed using the local reaction field (LRF) multiple expansion method [37]. All atoms beyond the 20 Å radius simulation sphere were held fixed to reduce computational costs [36], and solvent hydrogen bonds were maintained using the SHAKE algorithm [38].

Details regarding MD equilibration and production procedures for both the enzyme-bound and solvent-exposed (water) states can be found in our prior studies [26,27], which utilized the Q6 program [39]. Each equilibrated system underwent a total of 10 ns of MD simulations, conducted in five randomized replicas, each lasting 2 ns. A time step of 1 fs was employed, and no positional restraints were applied during these simulations. Specifically, for the free state, a weak harmonic restraint was employed to ensure that TYR inhibitors remained centered within their respective water simulation spheres.

*Binding Free Energies by the Linear Interaction Energy (LIE) Method*

Binding free energy calculations were conducted using a 10 ns duration of MD simulations from the production phase, employing the Linear Interaction Energy (LIE) method [39]. This method leverages ensembles representing both the bound and free states of a given ligand to determine their

free energy disparity [40–42]. The binding free energy ( $\Delta G_{LIE}$ ) for each TYR system was evaluated using the following LIE equation (Eq. 1):

$$\Delta G_{LIE} = \alpha \Delta U_{vdW} + \beta \Delta U_{ele} + \gamma \quad (1)$$

In this equation, the  $\alpha$  and  $\beta$  parameters serve as empirical scaling factors for the non-polar and polar components, respectively, contingent upon the chemical properties of the ligand [42]. These parameters can be derived from prior investigations ( $\alpha = 0.181$  and  $\beta = 0.33$ – $0.50$ ) [42], or alternatively through linear regression with experimental binding free energies ( $\Delta G_{EXP}$ ) (Eq. 2). The averages of van der Waals (vdW) and electrostatic (ele) interactions between the "bound" and "free" states were calculated using ensembles generated during MD production.

$$\Delta G_{EXP} = RT \ln IC_{50} + c \quad (2)$$

Here, the assay-specific constant ( $c$ ) relies on substrate concentration and the Michaelis-Menten constant [43]. Importantly, this constant does not impact relative free energies and can be implicitly incorporated into the optimized value of  $\gamma$  in Eq. 1.

## Results and Discussion

### *Molecular Docking and MD simulations*

Molecular docking and MD simulations are important techniques in the computational drug design process, collectively offering a comprehensive understanding of drug-target interactions. Molecular docking, by predicting the binding modes and affinities of potential drug candidates with target proteins, facilitates the identification of promising lead compounds. In contrast, MD simulations are used for exploring the dynamic behavior of these interactions, offering insights into the stability and conformational changes of drug-protein complexes over time. These combined approaches not only aid in optimizing drug candidates for enhanced binding but also accelerate the drug discovery process by reducing the number of costly experimental iterations. Consequently, molecular docking and MD continue to be indispensable tools in modern pharmaceutical research, contributing significantly to the development of innovative therapeutic agents [22,44–47].

It should be highlighted that arylpiperidine and arylpiperazine compounds are heterocyclic structures that possess diverse chemical functionalities, rendering them amenable to molecular modifications for targeted inhibition of TYR. According to Ferro et al. [19], the incorporation of aryl rings into these heterocyclic frameworks contributes to their binding affinity with the active site of the enzyme. Through systematic structural modifications, these researchers have been able to fine-tune the inhibitory potency and selectivity of these derivatives, enabling the development of lead compounds with enhanced bioactivity and reduced off-target effects. Besides, arylpiperidine and arylpiperazine derivatives exhibit diverse pharmacological activities beyond tyrosinase inhibition, making them attractive candidates for multifunctional therapeutic agents [48–51]. Very recently, while our study was in progress, an experimental and computational investigation involving compounds containing the 3-chloro-4-fluorophenyl group underscored the significance of this moiety in the inhibition of *Agaricus bisporus* TYR [52].

It is worth emphasizing that our molecular docking outcomes, employing the MVD package in conjunction with the MOLDOCK method [28], have demonstrated their efficacy in the context of TYR systems [23–27]. The MOLDOCK scoring function for each TYR inhibitor based on arylpiperidine and arylpiperazine moieties has been extracted and subsequently compared with experimental binding data (Table 3). In the case of the first group of compounds (without benzamide ring), L02–L12, a notable and positive correlation ( $r^2 = 0.73$ ) has been observed between the MOLDOCK scoring and experimental values. However, for arylpiperazine compounds (with benzamide ring), L13–L24, the correlation is notably weaker and negative ( $r^2 = -0.39$ ). These findings align with the expectations in the realm of molecular docking calculations. In many instances, docking algorithms can predict the appropriate binding modes but may not consistently rank various ligands based on their binding affinities [53].



**Table 3.** MOLDOCK scoring function and experimental binding free energy ( $\Delta G_{EXP}$ ) values for arylpiperidine (L02–L07) and arylpiperazine (L08–L24) based TYR inhibitors.

Inhibitor	MOLDOCK (kcal/mol)	$\Delta G_{EXP}$ (kcal/mol)	Inhibitor	MOLDOCK (kcal/mol)	$\Delta G_{EXP}$ (kcal/mol)
L02	-79.32	-5.58	L13	-95.49	-7.70
L03	-81.16	-6.53	L14	-101.05	-6.05
L04	-69.54	-5.02	L15	-102.65	-7.25
L05	-87.73	-6.55	L16	-96.04	-7.49
L06	-82.71	-6.32	L17	-100.97	-5.33
L07	-82.28	-6.68	L18	-102.06	-6.35
L08	-74.18	-5.77	L19	-97.34	-8.07
L09	-80.50	-6.15	L20	-102.81	-6.48
L10	-87.09	-6.09	L21	-106.33	-7.15
L11	-82.05	-6.40	L22	-99.78	-7.31
L12	-81.51	-6.91	L23	-100.74	-6.95
			L24	-97.81	-6.47

To carry out MD simulations after molecular docking is of paramount importance in drug discovery and structural biology. While molecular docking provides crucial insights into potential binding modes and initial binding affinities, MD simulations take this a step further by offering a dynamic view of the interactions between ligands and target proteins over time. This enables the exploration of structural changes, conformational dynamics, and the stability of the ligand-protein complex, which are often critical factors in understanding the true binding mechanism and predicting binding affinities accurately [54,55].

As detailed in the Computational Methods section, we conducted a total of five random replicas, each lasting 2 ns, utilizing the Q6 program [39]. This approach was adopted to generate ensembles that would enhance the understanding of the binding dynamics of arylpiperidine and arylpiperazine-based compounds with TYR. Our MD results reveal the robust stability of all simulated compounds within the catalytic site of TYR. Moreover, the structural characteristics of the TYR portion closely resemble those observed in prior computational investigations [26,27].

As can be observed in Table 4, it becomes evident that for the arylpiperidine group, the RMSD values span from 0.41±0.10 Å (L05) to 1.19±0.24 Å (L04), while for the arylpiperazine group, the RMSD values range from 0.39±0.10 Å (L20) to 0.97±0.30 Å (L24). These findings strongly indicate the effective stabilization of all simulated compounds within the TYR catalytic site in their respective complexes. Intriguingly, all inhibitors maintained the interaction between the fluorobenzyl group's fluorine atom and Cu<sup>2+</sup> ion (B) present in the TYR catalytic site, a feature akin to what is observed with natural substrates (L-Tyr and L-DOPA) as well as the KA inhibitor [56].

**Table 4.** Root Mean Square Deviation (RMSD) values, measured in angstroms (Å), pertain to the heavy atoms of inhibitors within the TYR enzyme complex.

Inhibitor	RMSD (Å)	Inhibitor	RMSD (Å)
L02	0.32±0.10	L13	0.71±0.33
L03	0.47±0.14	L14	0.95±0.52
L04	1.19±0.24	L15	0.70±0.27
L05	0.41±0.10	L16	0.82±0.28
L06	0.45±0.10	L17	0.55±0.15
L07	0.40±0.11	L18	0.79±0.21
L08	0.46±0.14	L19	0.79±0.28
L09	0.45±0.15	L20	0.39±0.10
L10	0.44±0.21	L21	0.67±0.17
L11	0.39±0.09	L22	0.52±0.11
L12	0.58±0.30	L23	0.52±0.11
		L24	0.97±0.30

Furthermore, this interaction aligns with the findings of Ferro et al. [19], whose research indicated that the electron density within the TYR active site corroborated the placement of the 4'-fluorobenzyl moiety between the two copper ions. Additionally, the aromatic ring was stabilized through stacking interactions with the residue His208 (Figure 2). The most potent arylpiperidine-based compound, L12, engages in a hydrogen interaction with Arg209 from TYR (Figure 2B), an interaction not observed in the case of L04 (Figure 2A). Additionally, as previously assessed [26,27], the CuDum model [33], employed for describing Cu<sup>2+</sup> ions, appropriately captured all the critical structural characteristics.



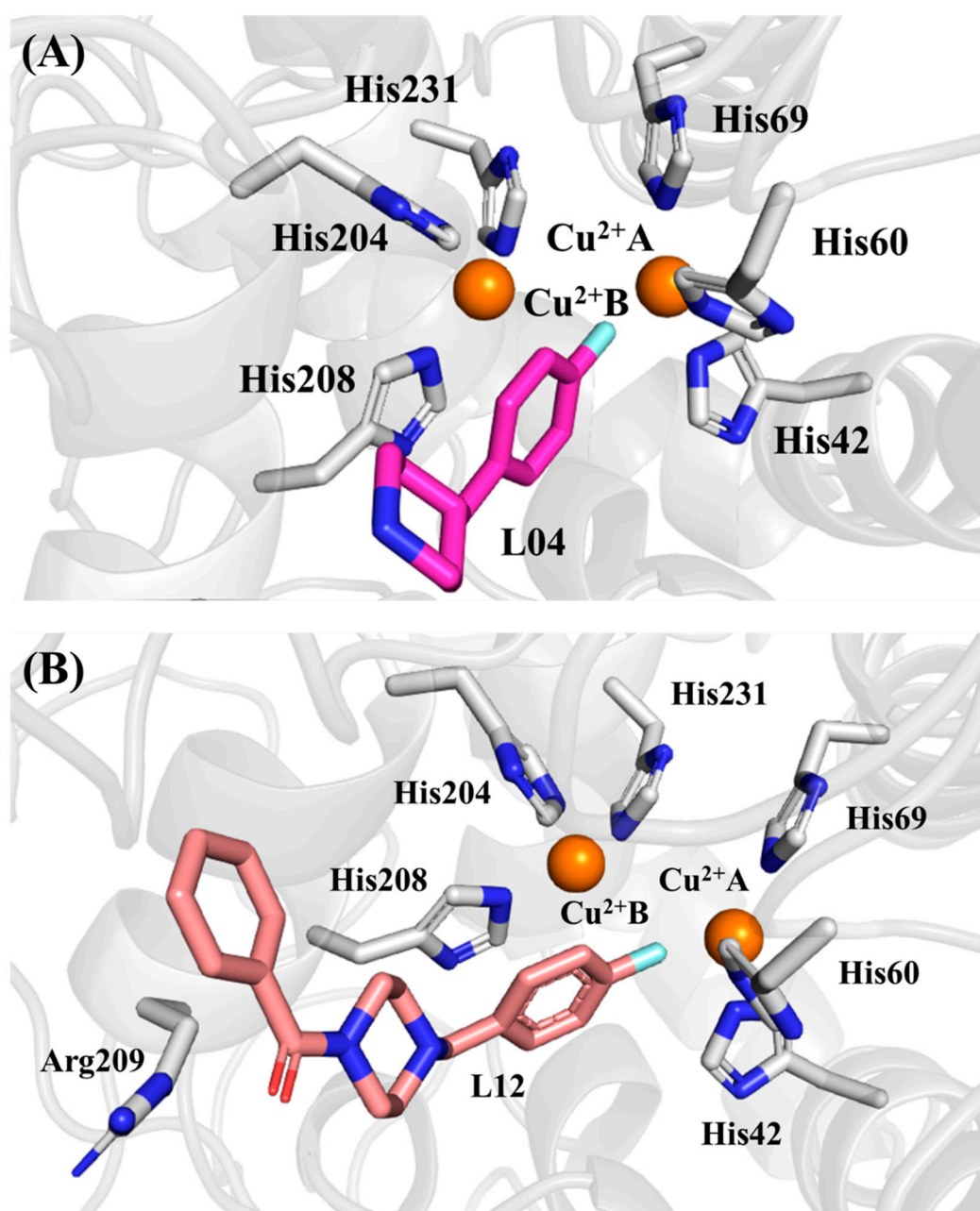


**Figure 2.** Representative MD structures of L04 (A) and L12 (B) inhibitors bound in the active site of the TYRBm.

Then, by considering the premises of the arylpiperidine group, it can be inferred that compounds interacting with the Arg209 residue possess enhanced inhibitory potential against the TYR enzyme. This interaction is evident in both the most potent inhibitor and the second least potent among the arylpiperazine compounds (Figure 3). The computational evidence presented here corroborates the observations made by Ferro et al. [19] regarding the mobility of Arg209, which facilitates the stabilization of bulky compounds within the active site of TYR.

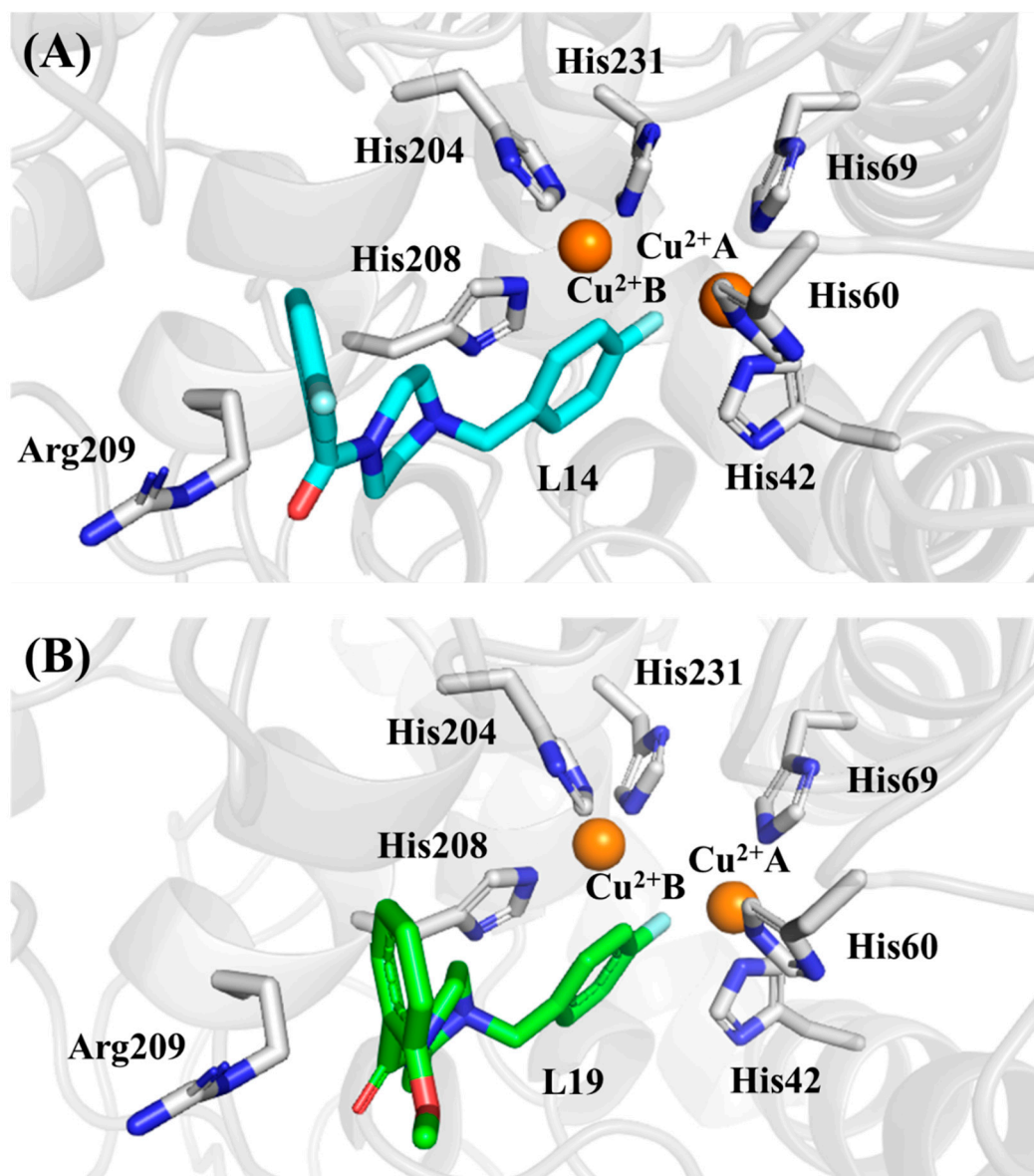


**Figure 3.** Representative MD structures of L14 (A) and L19 (B) inhibitors bound in the active site of the TYRBm.

### LIE calculations

The LIE method is an efficient computational approach used in drug design to estimate binding free energies between a ligand and its target protein [40–42,57]. This method provides a simplified yet accurate way to predict the changes in binding affinities by considering the energetic contributions from non-covalent interactions, such as van der Waals, electrostatic and hydrogen bonding interactions. One of the strengths of this method resides in its computational efficiency. Unlike more elaborate methods that require extensive sampling of conformational space [58], the LIE approach is suitable for high-throughput studies, virtual screening and lead optimization. It offers a balance between accuracy and computational cost, making it a valuable tool in the early stages of drug discovery [59].

In Table 5, we present the computed ligand-surrounding energies for arylpiperidine and arylpiperazine-based analogs, respectively. These values are derived from a comprehensive analysis of all MD simulations conducted for each inhibitor. Specifically, for the calculation of LIE-free energy values, we opted for a total of 10 ns of MD simulations for each TYR system. The empirical parameters  $\alpha$  and  $\beta$  were directly sourced from the literature [42], with additional details available in Table S1.

Notably, the optimized value of  $\gamma$  (set at -2.75) in the LIE equation for arylpiperazine was determined through linear fitting concerning  $\Delta G_{\text{EXP}}$ . Specifically, it was observed that omitting the inhibitors L02, L06, and L17 led to a notably improved correlation with  $\Delta G_{\text{EXP}}$ . Therefore, in all subsequent LIE discussions presented herein, these particular inhibitors have been intentionally excluded from the regression analysis. This approach mirrors the strategy employed by Carlsson et al. [60] and Vanga et al. [61] as well as previously for TYR systems [27].

**Table 5.** The calculated ( $\Delta G_{\text{LIE}}$ ) and experimental ( $\Delta G_{\text{EXP}}$ ) binding free energies for arylpiperidine and arylpiperazine-based TYR inhibitors. These values are expressed in kilocalories per mole (kcal/mol).

Inhibitor	$\Delta U_{\text{vdW}}$	$\Delta U_{\text{ele}}$	$\Delta G_{\text{LIE}}$	$\Delta G_{\text{EXP}}$
L03	-20.31	-6.72	-6.55	-6.53
L04	-11.86	-7.35	-5.00	-5.02
L05	-20.90	-6.82	-6.69	-6.55
L07	-20.93	-6.23	-6.44	-6.68
L08	-14.70	-8.92	-6.12	-5.77
L09	-20.09	-6.02	-6.20	-6.15
L10	-21.26	-5.54	-6.21	-6.09
L11	-22.37	-5.96	-6.59	-6.40
L12	-19.61	-7.55	-6.77	-6.91
L13	-23.53	-0.88	-7.36	-7.45
L14	-21.43	+1.13	-6.12	-5.85
L15	-24.26	-0.40	-7.28	-7.01
L16	-18.41	-2.52	-7.15	-7.25
L18	-25.38	+2.58	-6.20	-6.15
L19	-22.32	-2.17	-7.70	-7.81
L20	-18.21	-0.14	-6.09	-6.27
L21	-24.16	+0.48	-6.88	-6.92
L22	-21.87	-0.68	-6.94	-7.07
L23	-21.23	-0.28	-6.67	-6.72

L24

-23.65

+1.79

-6.34

-6.26

The LIE approach demonstrates the ability to reproduce the absolute binding free values for the arylpiperidine and arylpiperazine-based inhibitors within the experimental dataset ( $r^2 = 0.97$ ) (Figure 4). In our ensuing discussion, we will delve into the examination of the weakest inhibitor (L04) and the most potent one (L19) regarding TYR, aiming to pinpoint key characteristics that elucidate their binding discrepancies. Notably, the  $\Delta G_{\text{LIE}}$  value for L04 exceeds its experimental data by approximately 0.02 kcal/mol (-5.02 kcal/mol), while the  $\Delta G_{\text{LIE}}$  value for L19 exceeds its experimental value by roughly 0.11 kcal/mol (-7.81 kcal/mol). As previously proposed by Ferro et al. [19], the noteworthy TYR inhibitory activity exhibited by these arylpiperazine-based inhibitors can potentially be attributed to the presence of the benzamide ring. Consequently, exploring new interactions in this segment of TYR inhibitors can yield valuable insights into their inhibitory mechanisms. To decipher the energetic contributions of amino acid residues surrounding the TYR catalytic site, we conducted a residual decomposition analysis, encompassing both van der Waals (vdW) and electrostatic (ele) components as per the LIE equation. An interesting result concerning the electrostatic component can be observed among inhibitors L16 and L24, where those with substituent groups at the para position of the benzamide ring (L18, L21, and L24) exhibit positive electrostatic values: +2.58, +0.48, and +1.79 kcal/mol, respectively.

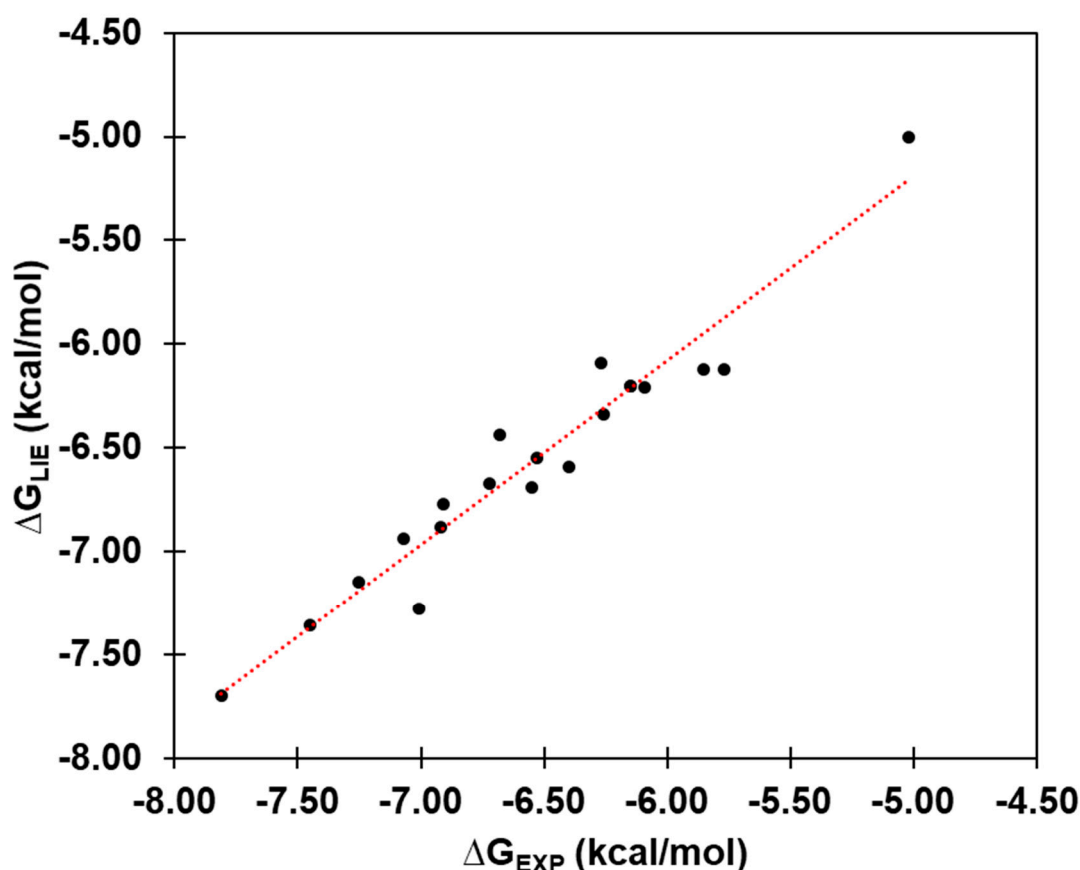


**Figure 4.** Linear regression model between the calculated ( $\Delta G_{\text{LIE}}$ ) and experimental ( $\Delta G_{\text{EXP}}$ ) binding free energy (in kcal/mol) for arylpiperidine and arylpiperazine-based inhibitors bound to TYR.

### Residual Decomposition Analysis

Residual decomposition analysis is a powerful computational technique used in binding free energy calculations to dissect and understand the contributions of individual molecular components

to the overall binding affinity between a ligand and its target protein. This approach provides insights into the specific interactions that drive ligand binding, shedding light on the underlying molecular mechanisms, serving as a valuable tool for validating binding hypotheses, explaining binding selectivity and suggesting ways to improve ligand binding. Its insights can facilitate the discovery of more potent and selective drug candidates, ultimately accelerating the drug development process [22,62–64].

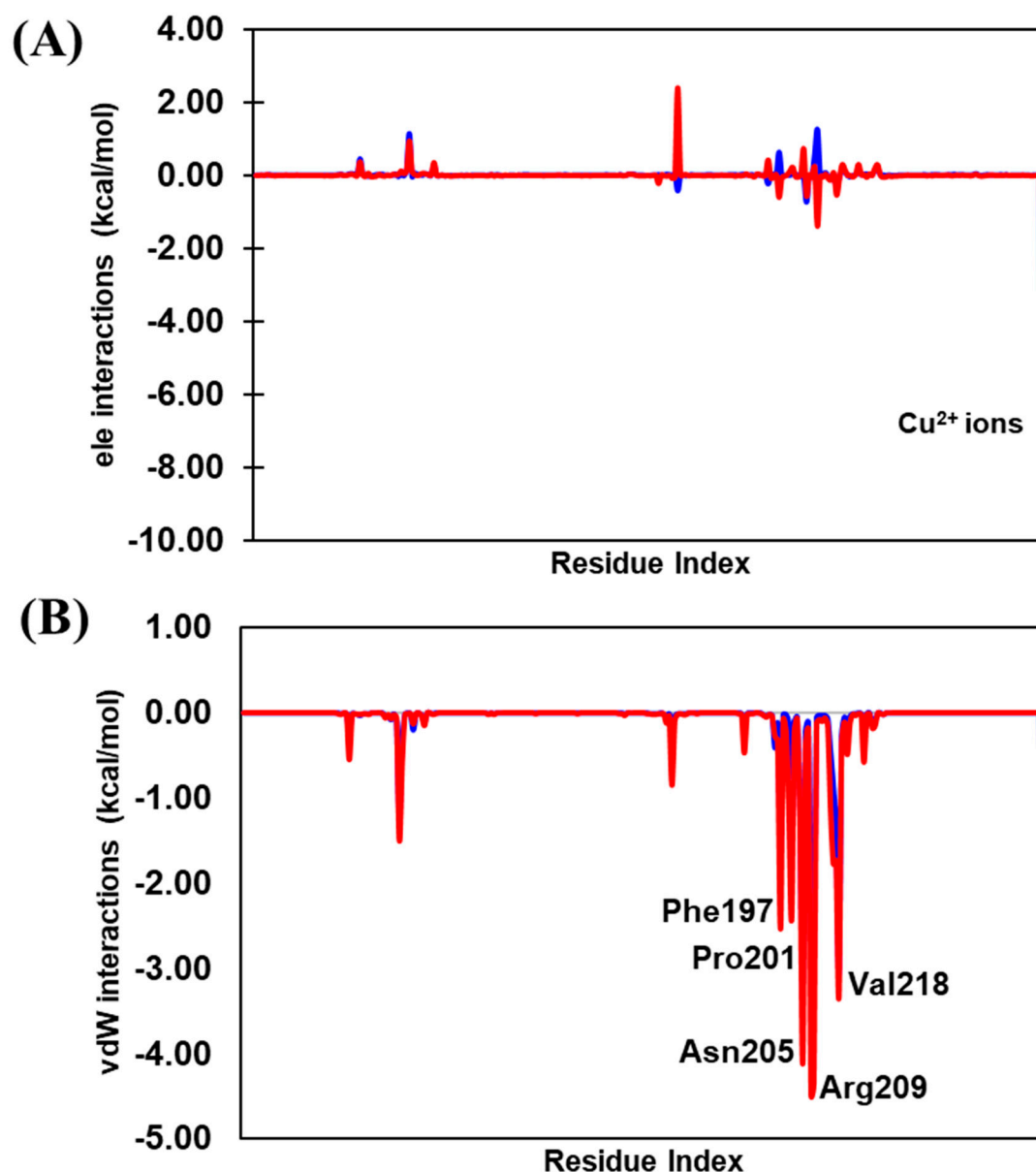


**Figure 5.** (A) electrostatic and (B) van der Waals (vdW) (in kcal/mol) energetic contributions over L04 (blue) and L19 (red) inhibitors used in the LIE calculations.

The average van der Waals (vdW) and electrostatic (ele) interaction energies for the TYR amino acid residues that significantly contribute to  $\Delta G_{LIE}$  are presented in Figure 4, considering both the most potent (L19, red lines) and weakest (L04, blue lines) TYR inhibitors. The values for others systems are reported in Table S2. In general, the electrostatic contributions from TYR residues exhibit minimal disparities between the L04 and L19 systems (Figure 4A). Notably, the electrostatic interaction with  $\text{Cu}^{2+}$  ions for L04 is -12.64 kcal/mol, whereas, for L19, it stands at -9.17 kcal/mol. Conversely, the vdW contributions undergo more substantial changes when transitioning from L04



to L19 inhibitors (Figure 4B). The most prominent differences are noticeable for Phe197, Pro201, Asn205, Arg209, and Val218, with values varying approximately by -0.94, -1.68, -0.91, -1.60, and -0.30 kcal/mol from L04 to L19 inhibitors, respectively (Figure 4B). Of particular interest is the interaction established between L19 and Arg209, characterized by a  $\pi$ -cation stacking contact between the amino acid sidechain and the benzamide ring of the arylpiperazine-based inhibitor.

Furthermore, it is confirmed that vdW interactions prevail over ele ones, even when considering all amino acids and Cu<sup>2+</sup> ions. The total ele contributions for the L04 and L16 systems are -9.45 and -5.54 kcal/mol, respectively, indicating a difference of approximately 4.00 kcal/mol. When considering the total vdW contributions, the systems exhibit -25.10 and -39.12 kcal/mol, respectively, signifying a difference of approximately -14.00 kcal/mol. These findings suggest that the inhibition of the TYR enzyme by these inhibitors is primarily driven by vdW interactions, underscoring the significance of the benzamide ring in the arylpiperidine and arylpiperazine-based inhibitors studied inhibitors.

## Conclusions

Here, we used computational techniques such as molecular docking, molecular dynamics (MD) simulations, and binding free energy calculations using the Linear Interaction Energy (LIE) method to investigate Tyrosinase inhibitors within the enzyme's active site. Our focus centered on a novel class of compounds containing arylpiperidine and arylpiperazine components. Throughout the computational analyses, all simulated compounds consistently exhibited stability within the catalytic site of TYR, maintaining the key interactions with essential residues and Cu<sup>2+</sup> ions. The interaction involving the fluorine atom of the fluorobenzyl group and the copper ion remained stable during MD simulations. The results also show that van der Waals interactions due to the presence of the benzamide group are important for the stabilization of the inhibitors. Furthermore, our results corroborate the accuracy of the LIE approach in estimating binding free energies. In general, this investigation provides valuable insights into the understanding of TYR inhibition and offers guidance for the development of potential therapeutic agents.

**Funding:** This research was funded by the National Council for Scientific and Technological Development (process #440053/2022-6). L.S.M. (process #88882.445391/2019-01) thanks the CAPES financial agency for providing scholarships during the development of this project.

**Acknowledgments:** This project has received authorization to utilize computational resources from several esteemed institutions: South African Centre for High-Performance Computing (<https://www.chpc.ac.za/>), Hippo at the University of KwaZulu-Natal (<https://astro.ukzn.ac.za/~hippo/>) and High-Performance Computing Center of Federal University of Pará (<https://www.ccad.ufpa.br/>). The authors would like to express their gratitude to PROPESP/UFGA for generously covering the publication fee.

**Conflicts of Interest:** The authors declare no conflict of interest.

## References

1. Chang, T.S. An Updated Review of Tyrosinase Inhibitors. *Int. J. Mol. Sci.* **2009**, *10*, 2440–2475, doi:10.3390/ijms10062440.
2. Kim, Y.J.; Uyama, H. Tyrosinase Inhibitors from Natural and Synthetic Sources: Structure, Inhibition Mechanism and Perspective for the Future. *Cell. Mol. Life Sci.* **2005**, *62*, 1707–1723, doi:10.1007/s00018-005-5054-y.
3. Saghaie, L.; Pourfarzam, M.; Fassihi, A.; Sartippour, B. Synthesis and Tyrosinase Inhibitory Properties of Some Novel Derivatives of Kojic Acid. *Res Pharm Sci* **2013**, *8*, 233–242.
4. D'Mello, S.; Finlay, G.; Baguley, B.; Askarian-Amiri, M. Signaling Pathways in Melanogenesis. *Int. J. Mol. Sci.* **2016**, *17*, 1144, doi:10.3390/ijms17071144.
5. Carballo-Carbajal, I.; Laguna, A.; Romero-Giménez, J.; Cuadros, T.; Bové, J.; Martínez-Vicente, M.; Parent, A.; Gonzalez-Sepulveda, M.; Peñuelas, N.; Torra, A.; et al. Brain Tyrosinase Overexpression Implicates Age-Dependent Neuromelanin Production in Parkinson's Disease Pathogenesis. *Nat. Commun.* **2019**, *10*, doi:10.1038/s41467-019-08858-y.
6. Kamo, H.; Kawahara, R.; Simizu, S. Tyrosinase Suppresses Vasculogenic Mimicry in Human Melanoma Cells. *Oncol. Lett.* **2022**, *23*, 169, doi:10.3892/ol.2022.13289.



7. Brenner, M.; Hearing, V.J. The Protective Role of Melanin Against UV Damage in Human Skin†. *Photochem. Photobiol.* **2008**, *84*, 539–549, doi:10.1111/j.1751-1097.2007.00226.x.
8. Del Bino, S.; Duval, C.; Bernerd, F. Clinical and Biological Characterization of Skin Pigmentation Diversity and Its Consequences on UV Impact. *Int. J. Mol. Sci.* **2018**, *19*, 2668, doi:10.3390/ijms19092668.
9. Sánchez-Ferrer, Á.; Neptuno Rodríguez-López, J.; García-Cánovas, F.; García-Carmona, F. Tyrosinase: A Comprehensive Review of Its Mechanism. *Biochim. Biophys. Acta - Protein Struct. Mol. Enzymol.* **1995**, *1247*, 1–11, doi:10.1016/0167-4838(94)00204-T.
10. Pillaiyar, T.; Manickam, M.; Namasivayam, V. Skin Whitening Agents: Medicinal Chemistry Perspective of Tyrosinase Inhibitors. *J. Enzyme Inhib. Med. Chem.* **2017**, *32*, 403–425, doi:10.1080/14756366.2016.1256882.
11. Solano, F. On the Metal Cofactor in the Tyrosinase Family. *Int. J. Mol. Sci.* **2018**, *19*, 633, doi:10.3390/ijms19020633.
12. Cabanes, J.; Chazarra, S.; Garcia-Carmona, F. Kojic Acid, a Cosmetic Skin Whitening Agent, Is a Slow-Binding Inhibitor of Catecholase Activity of Tyrosinase. *J. Pharm. Pharmacol.* **2011**, *46*, 982–985, doi:10.1111/j.2042-7158.1994.tb03253.x.
13. Uchino, K.; Nagawa, M.; Tonosaki, Y.; Oda, M.; Fukuchi, A. Kojic Acid as an Anti-Speck Agent. *Agric. Biol. Chem.* **1988**, *52*, 2609–2610, doi:10.1080/00021369.1988.10869087.
14. Saruno, R.; Kato, F.; Ikeno, T. Kojic Acid, a Tyrosinase Inhibitor from *Aspergillus Albus*. *Agric. Biol. Chem.* **1979**, *43*, 1337–1338, doi:10.1080/00021369.1979.10863620.
15. Brtko, J.; Rondahl, L.; Ficková, M.; Hudecová, D.; Eybl, V.; Uher, M. Kojic Acid and Its Derivatives: History and Present State of Art. *Cent. Eur. J. Public Health* **2004**, *12 Suppl*, S16-8.
16. Burdock, G.A.; Soni, M.G.; Carabin, I.G. Evaluation of Health Aspects of Kojic Acid in Food. *Regul. Toxicol. Pharmacol.* **2001**, *33*, 80–101, doi:10.1006/rtph.2000.1442.
17. Chen, W.-C.; Tseng, T.-S.; Hsiao, N.-W.; Lin, Y.-L.; Wen, Z.-H.; Tsai, C.-C.; Lee, Y.-C.; Lin, H.-H.; Tsai, K.-C. Discovery of Highly Potent Tyrosinase Inhibitor, T1, with Significant Anti-Melanogenesis Ability by Zebrafish in Vivo Assay and Computational Molecular Modeling. *Sci. Rep.* **2015**, *5*, 7995, doi:10.1038/srep07995.
18. Hashemi, S.M.; Emami, S. Kojic Acid-Derived Tyrosinase Inhibitors: Synthesis and Bioactivity. *Pharm. Biomed. Res.* **2015**, *1*, 1–17, doi:10.18869/acadpub.pbr.1.1.1.
19. Ferro, S.; Deri, B.; Germanò, M.P.; Gitto, R.; Ielo, L.; Buemi, M.R.; Certo, G.; Vittorio, S.; Rapisarda, A.; Pazy, Y.; et al. Targeting Tyrosinase: Development and Structural Insights of Novel Inhibitors Bearing Arylpiperidine and Arylpiperazine Fragments. *J. Med. Chem.* **2018**, *61*, 3908–3917, doi:10.1021/acs.jmedchem.7b01745.
20. Zolghadri, S.; Bahrami, A.; Hassan Khan, M.T.; Munoz-Munoz, J.; Garcia-Molina, F.; Garcia-Canovas, F.; Saboury, A.A. A Comprehensive Review on Tyrosinase Inhibitors. *J. Enzyme Inhib. Med. Chem.* **2019**, *34*, 279–309, doi:10.1080/14756366.2018.1545767.
21. Chang, T.-S. An Updated Review of Tyrosinase Inhibitors. *Int. J. Mol. Sci.* **2009**, *10*, 2440–2475, doi:10.3390/ijms10062440.
22. Sabe, V.T.; Ntombela, T.; Jhamba, L.A.; Maguire, G.E.M.; Govender, T.; Naicker, T.; Kruger, H.G. Current Trends in Computer Aided Drug Design and a Highlight of Drugs Discovered via Computational Techniques: A Review. *Eur. J. Med. Chem.* **2021**, *224*, 113705, doi:10.1016/j.ejmech.2021.113705.
23. Brasil, E.M.; Canavieira, L.M.; Cardoso, É.T.C.; Silva, E.O.; Lameira, J.; Nascimento, J.L.M.; Eifler-Lima, V.L.; Macchi, B.M.; Sriram, D.; Bernhardt, P. V.; et al. Inhibition of Tyrosinase by 4 H -Chromene Analogs: Synthesis, Kinetic Studies, and Computational Analysis. *Chem. Biol. Drug Des.* **2017**, *90*, 804–810, doi:10.1111/cbdd.13001.
24. Lima, C.R.; Silva, J.R.A.; De Tássia Carvalho Cardoso, É.; Silva, E.O.; Lameira, J.; Do Nascimento, J.L.M.; do Socorro Barros Brasil, D.; Alves, C.N. Combined Kinetic Studies and Computational Analysis on Kojic Acid Analogs as Tyrosinase Inhibitors. *Molecules* **2014**, *19*, 9591–9605, doi:10.3390/molecules19079591.
25. Canavieira, L.M.; Brasil, E.M.; Silva, T. de M. e; Borges, R. dos S.; Silva, J.R.A.; Lameira, J.; Bernhardt, P. V.; Williams, C.M.; Alves, C.N. Experimental and Theoretical Approaches for the Development of 4H-Chromene Derivatives as Inhibitors of Tyrosinase. *Mol. Simul.* **2021**, *47*, 762–770, doi:10.1080/08927022.2021.1926455.
26. Martins, L.S.; Lameira, J.; Kruger, H.G.H.G.; Alves, C.N.; Silva, J.R.A. Evaluating the Performance of a Non-Bonded Cu<sup>2+</sup> Model Including Jahn–Teller Effect into the Binding of Tyrosinase Inhibitors. *Int. J. Mol. Sci.* **2020**, *21*, 4783, doi:10.3390/ijms21134783.
27. Martins, L.S.; Gonçalves, R.W.A.; Moraes, J.J.S.; Alves, C.N.; Silva, J.R.A. Computational Analysis of Triazole-Based Kojic Acid Analogs as Tyrosinase Inhibitors by Molecular Dynamics and Free Energy Calculations. *Molecules* **2022**, *27*, 8141, doi:10.3390/molecules27238141.
28. Thomsen, R.; Christensen, M.H. MolDock: A New Technique for High-Accuracy Molecular Docking. *J. Med. Chem.* **2006**, *49*, 3315–3321, doi:10.1021/jm051197e.

29. Jorgensen, W.; Maxwell, D.; Tirado-rives, J. Development and Testing of the OPLS All-Atom Force Field on Conformational Energetics and Properties of Organic Liquids. *J. Am. Chem. Soc.* **1996**, *118*, 11225–11236, doi:10.1021/ja9621760.
30. Jorgensen, W.L.; Chandrasekhar, J.; Madura, J.D.; Impey, R.W.; Klein, M.L. Comparison of Simple Potential Functions for Simulating Liquid Water. *J. Chem. Phys.* **1983**, *79*, 926–935, doi:10.1063/1.445869.
31. Schrödinger Schrödinger Release 2020-1: MacroModel, Schrödinger, LLC, New York, NY, 2020.
32. Mohamadi, F.; Richards, N.G.J.; Guida, W.C.; Liskamp, R.; Lipton, M.; Caufield, C.; Chang, G.; Hendrickson, T.; Still, W.C. MacroModel?An Integrated Software System for Modeling Organic and Bioorganic Molecules Using Molecular Mechanics. *J. Comput. Chem.* **1990**, *11*, 440–467, doi:10.1002/jcc.540110405.
33. Liao, Q.; Kamerlin, S.C.L.; Strodel, B. Development and Application of a Nonbonded Cu 2+ Model That Includes the Jahn–Teller Effect. *J. Phys. Chem. Lett.* **2015**, *6*, 2657–2662, doi:10.1021/acs.jpcllett.5b01122.
34. Olsson, M.H.M.; Søndergaard, C.R.; Rostkowski, M.; Jensen, J.H. PROPKA3: Consistent Treatment of Internal and Surface Residues in Empirical PKa Predictions. *J. Chem. Theory Comput.* **2011**, *7*, 525–537, doi:10.1021/ct100578z.
35. King, G.; Warshel, A. A Surface Constrained All-atom Solvent Model for Effective Simulations of Polar Solutions. *J. Chem. Phys.* **1989**, *91*, 3647–3661, doi:10.1063/1.456845.
36. Marelus, J.; Kolmodin, K.; Feierberg, I.; Åqvist, J. Q: A Molecular Dynamics Program for Free Energy Calculations and Empirical Valence Bond Simulations in Biomolecular Systems. *J. Mol. Graph. Model.* **1998**, *16*, 213–225, doi:10.1016/S1093-3263(98)80006-5.
37. Diaz, L.; Bujons, J.; Delgado, A.; Gutierrez-de-Terán, H.; Aqvist, J. Computational Prediction of Structure-Activity Relationships for the Binding of Aminocyclitols to Beta-Glucocerebrosidase. *J. Chem. Inf. Model* **2011**, *51*, 601–611, doi:10.1021/ci100453a.
38. Ryckaert, J.-P.; Ciccotti, G.; Berendsen, H.J.C. Numerical Integration of the Cartesian Equations of Motion of a System with Constraints: Molecular Dynamics of n-Alkanes. *J. Comput. Phys.* **1977**, *23*, 327–341, doi:https://doi.org/10.1016/0021-9991(77)90098-5.
39. Bauer, P.; Barrozo, A.; Purg, M.; Amrein, B.A.; Esguerra, M.; Wilson, P.B.; Major, D.T.; Åqvist, J.; Kamerlin, S.C.L. Q6: A Comprehensive Toolkit for Empirical Valence Bond and Related Free Energy Calculations. *SoftwareX* **2018**, *7*, 388–395, doi:10.1016/j.softx.2017.12.001.
40. Gutiérrez-de-Terán, H.; Åqvist, J. Linear Interaction Energy: Method and Applications in Drug Design. In: 2012; pp. 305–323.
41. Åqvist, J.; Marelus, J. The Linear Interaction Energy Method for Predicting Ligand Binding Free Energies. *Comb. Chem. High Throughput Screen.* **2001**, *4*, 613–626, doi:10.2174/1386207013330661.
42. Hansson, T.; Marelus, J.; Åqvist, J. Ligand Binding Affinity Prediction by Linear Interaction Energy Methods. *J. Comput. Aided. Mol. Des.* **1998**, 27–35, doi:10.1023/A:1007930623000.
43. Yung-Chi, C.; Prusoff, W.H. Relationship between the Inhibition Constant (KI) and the Concentration of Inhibitor Which Causes 50 per Cent Inhibition (I50) of an Enzymatic Reaction. *Biochem. Pharmacol.* **1973**, *22*, 3099–3108, doi:10.1016/0006-2952(73)90196-2.
44. Honarparvar, B.; Govender, T.; Maguire, G.E.M.; Soliman, M.E.S.; Kruger, H.G. Integrated Approach to Structure-Based Enzymatic Drug Design: Molecular Modeling, Spectroscopy, and Experimental Bioactivity. *Chem. Rev.* **2014**, *114*, 493–537, doi:10.1021/cr300314q.
45. Ferreira, L.G.; Dos Santos, R.N.; Oliva, G.; Andricopulo, A.D. *Molecular Docking and Structure-Based Drug Design Strategies*; 2015; Vol. 20; ISBN 1420-3049.
46. Gani, O.A.B.S.M. Signposts of Docking and Scoring in Drug Design. *Chem. Biol. Drug Des.* **2007**, *70*, 360–365, doi:10.1111/j.1747-0285.2007.00571.x.
47. Batool, M.; Ahmad, B.; Choi, S. A Structure-Based Drug Discovery Paradigm. *Int. J. Mol. Sci.* **2019**, *20*, 2783, doi:10.3390/ijms20112783.
48. Yi, Y.; Yang, S.; Liu, Y.; Yin, B.; Zhao, Z.; Li, G.; Huang, Z.; Chen, L.; Liu, F.; Shang, R.; et al. Antibiotic Resistance and Drug Modification: Synthesis, Characterization and Bioactivity of Newly Modified Potent Pleuromutilin Derivatives with a Substituted Piperazine Moiety. *Bioorg. Chem.* **2023**, *132*, 106353, doi:https://doi.org/10.1016/j.bioorg.2023.106353.
49. Ji, Q.; Li, B.; Chu, Y.; Wu, H.; Du, C.; Xu, Y.; Shen, Y.; Deng, J. Design, Synthesis and Biological Evaluation of Novel Diazaspirodecane Derivatives Containing Piperidine-4-Carboxamide as Chitin Synthase Inhibitors and Antifungal Agents. *Bioorg. Chem.* **2021**, *114*, 105108, doi:https://doi.org/10.1016/j.bioorg.2021.105108.
50. Yar, M.; Shahzadi, L.; Farooq, A.; Jalil Imran, S.; Cerón-Carrasco, J.P.; den-Haan, H.; Kumar, S.; Peña-García, J.; Pérez-Sánchez, H.; Grycova, A.; et al. In Vitro Modulatory Effects of Functionalized Pyrimidines and Piperidine Derivatives on Aryl Hydrocarbon Receptor (AhR) and Glucocorticoid Receptor (GR) Activities. *Bioorg. Chem.* **2017**, *71*, 285–293, doi:https://doi.org/10.1016/j.bioorg.2017.02.013.

51. Hu, J.; Gao, M.; Zhang, Y.; Wang, Y.; Qiao, Z.; Zhang, W.; Wang, Q.; Yan, L.; Qian, H. Novel Piperazine Urea Derivatives as Highly Potent Transient Receptor Potential Vanilloid 1 (TRPV1) Antagonists. *Bioorg. Chem.* **2021**, *115*, 105229, doi:https://doi.org/10.1016/j.bioorg.2021.105229.
52. Mirabile, S.; Ielo, L.; Lombardo, L.; Ricci, F.; Gitto, R.; Germanò, M.P.; Pace, V.; De Luca, L. Leveraging the 3-Chloro-4-Fluorophenyl Motif to Identify Inhibitors of Tyrosinase from *Agaricus Bisporus*. *Int. J. Mol. Sci.* **2023**, *24*, 7944, doi:10.3390/ijms24097944.
53. Warren, G.L.; Andrews, C.W.; Capelli, A.-M.; Clarke, B.; LaLonde, J.; Lambert, M.H.; Lindvall, M.; Nevins, N.; Semus, S.F.; Senger, S.; et al. A Critical Assessment of Docking Programs and Scoring Functions. *J. Med. Chem.* **2006**, *49*, 5912–5931, doi:10.1021/jm050362n.
54. De Vivo, M.; Cavalli, A. Recent Advances in Dynamic Docking for Drug Discovery. *WIREs Comput. Mol. Sci.* **2017**, *7*, 1–10, doi:10.1002/wcms.1320.
55. Liu, X.; Shi, D.; Zhou, S.; Liu, H.; Liu, H.; Yao, X. Molecular Dynamics Simulations and Novel Drug Discovery. *Expert Opin. Drug Discov.* **2018**, *13*, 23–37, doi:10.1080/17460441.2018.1403419.
56. Deri, B.; Kanteev, M.; Goldfeder, M.; Lecina, D.; Guallar, V.; Adir, N.; Fishman, A. The Unravelling of the Complex Pattern of Tyrosinase Inhibition. *Sci. Rep.* **2016**, *6*, 34993, doi:10.1038/srep34993.
57. Almlöf, M.; Carlsson, J.; Åqvist, J. Improving the Accuracy of the Linear Interaction Energy Method for Solvation Free Energies. *J. Chem. Theory Comput.* **2007**, *3*, 2162–2175, doi:10.1021/ct700106b.
58. Limongelli, V. Ligand Binding Free Energy and Kinetics Calculation in 2020. *Wiley Interdiscip. Rev. Comput. Mol. Sci.* **2020**, *10*, 1–32, doi:10.1002/wcms.1455.
59. Murcko, M.A. Computational Methods to Predict Binding Free Energy in Ligand-Receptor Complexes. *J. Med. Chem.* **1995**, *38*, 4953–4967, doi:10.1021/jm00026a001.
60. Carlsson, J.; Boukharta, L.; Åqvist, J. Combining Docking, Molecular Dynamics and the Linear Interaction Energy Method to Predict Binding Modes and Affinities for Non-Nucleoside Inhibitors to HIV-1 Reverse Transcriptase. *J. Med. Chem.* **2008**, *51*, 2648–2656, doi:10.1021/jm7012198.
61. Vanga, S.R.; Sävmarker, J.; Ng, L.; Larhed, M.; Hallberg, M.; Åqvist, J.; Hallberg, A.; Chai, S.Y.; Gutiérrez-De-Terán, H. Structural Basis of Inhibition of Human Insulin-Regulated Aminopeptidase (IRAP) by Aryl Sulfonamides. *ACS Omega* **2018**, *3*, 4509–4521, doi:10.1021/acsomega.8b00595.
62. Gurung, A.B.; Ali, M.A.; Lee, J.; Farah, M.A.; Al-Anazi, K.M. An Updated Review of Computer-Aided Drug Design and Its Application to COVID-19. *Biomed Res. Int.* **2021**, *2021*, 1–18, doi:10.1155/2021/8853056.
63. Schneider, G. Future De Novo Drug Design. *Mol. Inform.* **2014**, *33*, 397–402, doi:10.1002/minf.201400034.
64. Mobley, D.L.; Dill, K.A. Binding of Small-Molecule Ligands to Proteins: “What You See” Is Not Always “What You Get.” *Structure* **2009**, *17*, 489–498, doi:10.1016/j.str.2009.02.010.

**Disclaimer/Publisher’s Note:** The statements, opinions and data contained in all publications are solely those of the individual author(s) and contributor(s) and not of MDPI and/or the editor(s). MDPI and/or the editor(s) disclaim responsibility for any injury to people or property resulting from any ideas, methods, instructions or products referred to in the content.